Eng. & Tech. Journal, Vol.28, No.18, 2010

Analysis of the Performance of Flexible Pavement under the Effect of Wheel and Thermal Loads

Dr. Mohammed Y. Fattah * Shayma'a Abd. El-Ghany * & Ahmed S. Abdaljabbar*

Received on: 18 / 1 / 2010
Accepted on: 2 / 9 / 2010

Abstract

One of the major sources of distress in roads is the cracks that appear in flexible asphalt pavements. Combined wheel and thermal load induced cracking in the form of bottom-up and top-down fatigue cracking.

In this paper, combined effect of wheel loads and temperature is considered in finite element analysis of flexible pavement layers. The heat flow equations are derived and the program (ANSYS V 5.4) is utilized to carry out the analysis. The subgrade layer is modeled as an elasto-plastic material following Drucker–Prager model for yielding of the isotropic material, while both the asphalt and base layers are considered elastic. Three different thicknesses for the asphalt layer are tried; namely, 0.05 m, 0.10 m and 0.15 m, respectively. A temperature rise of 40^{o}C was considered in addition to wheel pressures.

It was found that an increase of wheel pressure from (500) to (700) kN/m^{2} leads to increase in vertical displacement of about (4– 8)%. This increase becomes (10– 22%) when the wheel pressure becomes 1000 kN/m^{2}. The temperature rise leads to decrease in the effect of wheel pressure because temperature leads to expansion (upward movement) reverse to wheel load effect.

The effect of wheel load is transmitted directly to the underlying subgrade within the wheel zone. The deformed zone under the wheel becomes larger when the load increases. The maximum displacement increases by about (24%) when the load is duplicated.

Keywords: Flexible pavement, wheel loads, temperature, finite elements.

تحليل أداء التبليط الاسفلتي المرن تحت تأثير أحمال العجلات و الحرارة

الخلاصة

تعتبر التشققات واحدا من المصادر الرئيسية للأخطار في الطرق و التي تظهر في التبليط الاسفلتي المرن. يسبب الحمل المركب من العجلات و الحرارة تشققات تأخذ شكل تشققات كلل من الأسفل للأعلى و من الأعلى للأسفل.

في هذا البحث تم أخذ التأثير المركب لأحمال العجلات و الحرارة في التحليل بطريقة العناصر المحددة لطبقات التبليط الأسفلتي المرن. تم اشتقاق المعادلات الخاصة بانتقال الحرارة و أستعمل برنامج الحاسبة (ANSYS V 5.4) للقيام بالتحليل. و قد تم تمثيل طبقة التربة التحتية كمادة مرنة لدنة تتبع نموذج الاذعان المتماثل لدركر-براغر بينما مثلت مادة طبقة الأساس و المادة الاسفلتية تمثيلا مرنا. و جربت ثلاث

* Building & Construction Engineering Department, University of Technology/Baghdad

https://doi.org/10.30684/etj.28.18.14
2412-0758/University of Technology-Iraq, Baghdad, Iraq
This is an open access article under the CC BY 4.0 license http://creativecommons.org/licenses/by/4.0

قيم لسمك طبقة الاسفلت و هي 0.05 م و 0.10 م و 0.15 م ، و تم اعتبار ارتفاع درجة الحرارة بمقدار 40^{o} مئوية اضافة الى ضغوط العجلات.

و قد وجد أن ارتفاع ضغط العجلة من (500) الى (700) كيلونيوتن/م^{2} يؤدي الى زيادة الازاحة الشاقولية بحدود (4-8)% ، و تصبح هذه الزيادة بحدود (10-22)% عندما يصبح ضغط العجلة (1000) كيلونيوتن/م^{2}. ان ارتفاع درجة الحرارة يؤدي الى تقليل تأثير ضغط العجلة لأن الحرارة تؤدي الى تمدد (حركة للأعلى) معاكس لتأثير حمل العجلة.

ان تأثير حمل العجلة ينتقل مباشرة الى طبقة التربة التحتية ضمن منطقة العجلة و تصبح المنطقة المشوهة تحت العجلة أكبر عند زيادة الحمل. و تزداد الازاحة القصوى بمقدار حوالي (24%) عند مضاعفة الحمل.

Introduction

Temperature has a significant effect on the stiffness as well as the fatigue and permanent deformation resistance of asphalt mixtures. It is therefore quite obvious that accurate knowledge of the temperature distribution in the pavement should be available in order to allow realistic analyses of the stresses and strains in asphalt pavements to be made. Furthermore moisture has a significant effect on the stiffness and strength characteristics of unbound materials and soils.

Temperature Distribution in Pavement

The temperature distribution in the pavement layers can vary significantly during the day and during the seasons of the year. Figure 1 shows the temperature distribution during a hot spring and a hot summer day. One should realize that the surface temperatures can easily be 5^{0}C higher than the temperatures measured at 10 mm below the pavement surface. Figure 2 shows the temperature gradient that exists over the asphalt layer thickness in case of the hot summer day shown in Figure 1. Because the stiffness of asphalt layers changes with temperature, allowance must be made in the design of these pavements for the different temperatures at which they will operate (Pavement Design Manual, 2005).

From these figures, it is clear that assuming a constant temperature over the thickness of the asphalt layer is far from reality unless one is dealing with thin asphalt layers. Furthermore, the total asphalt thickness is commonly made of different types of asphalt mixtures, especially in case the total thickness is larger than 100 mm, which implies that even when the temperature is constant over the entire thickness, different stiffness values will be found for the different layers of which the total asphalt thickness is made of. Van Gurp (1995) presented a method to deal with temperature variations over the total asphalt thickness. He divided the total thickness into three sub-layers (Figure 3) and defined an equivalent asphalt thickness, $h_{1,eq}$ in the way as described in Figure 4. This equivalent thickness has a modulus value equal to the modulus of the third sub-layer.

The equivalent asphalt thickness is calculated as follows:

$$h_{1,eq} = (h_1/4)*[(n_1^2 n_2^2 + 64 n_1 n_2^2 + 110 n_1 n_2 + 16 n_2^2 + 64 n_2 + 1)(n_1 n_2 + 2 n_2 + 1)]^{0.33}$$

PDF created with pdfFactory Pro trial version www.pdffactory.com

Where: h1, eq = equivalent total asphalt thickness with stiffness $E_{1,3}$:

$$n_1 = \frac{E_{1,1}}{E_{1,2}}$$ And

$$n_2 = \frac{E_{1,2}}{E3}$$

This equation is valid under the assumption that $h_{1,1}$ = ¼ h_1 and $h_{1,3}$ = ¼ h_1 and that the temperature is uniformly distributed over each of the sub-layers. The mean temperature of each sub-layer is used to calculate the modulus of that sublayer.

Reflective cracking

Reflective cracking cannot be analyzed by means of linear elastic multi layer theory. The finite element method needs to be used in order to be able to model the effects of discontinuities like cracks. Furthermore, principles of fracture mechanics need to be used in order to be able to analyze the rate at which the crack will propagate through the asphalt layer. In principle, there are two mechanisms that are responsible for the crack propagation being temperature effects and traffic loads. Both effects are schematically represented in Figures 5, 6 and 7.

Before one is going in detailed finite element analyses, it might be wise to analyze the crack reflection due to traffic loads first of all with a simplified procedure. Such a simplified procedure is presented hereafter.

A general applicable simple design system has been developed by Lytton (1989); this method is based on the propagation of cracks in fully supported beams.

Alkaiss and Al-Maliky (2009) studied the behavior of flexible pavement under wheel and thermal loading conditions using the finite element method. They investigated the stress distribution within the asphalt concrete pavement that influences the direction of crack propagation. The results showed that a maximum stress intensity factor value is obtained at surface and then decrease with depth about (0.75 of asphalt layer thickness) due to reduction in temperature in asphalt layer, which indicates that crack will initiate at surface and extend throughout asphalt layer. The horizontal stress for both top and bottom layers increases with the variation of thermal coefficient expansion factor. High values of stresses at top surface of asphalt layer due to high contact stress were induced under wheel and thermal load conditions.

Heat Flow Fundamentals

The first law of thermodynamics states that thermal energy is conserved. Specializing this to a differential control volume:

$$\rho c\left(\frac{\partial T}{\partial t} + \{v\}^T \{L\}T\right) + \{L\}^T \{q\} = \ddot{q}$$

….(1)

where:

ρ = density,

c = specific heat,

T = temperature (=T(x, y, z, t)), and

t = time

PDF created with pdfFactory Pro trial version www.pdffactory.com

$$\{L\} = \begin{Bmatrix} \frac{\partial}{\partial x} \\ \frac{\partial}{\partial y} \\ \frac{\partial}{\partial z} \end{Bmatrix} = \text{vector operator}$$

$$\{v\} = \begin{Bmatrix} v_x \\ v_y \\ v_z \end{Bmatrix}$$

= velocity vector for mass transport of heat.

{q} = heat flux vector (output as TFX, TFY, and TFZ)

$\ddot{q}$= heat generation rate per unit volume.

Next, Fourier's law is used to relate the heat flux vector to the thermal gradients:

$$\{q\} = -[D]\{L\}T$$

where:

$$[D] = \begin{bmatrix} K_{xx} & 0 & 0 \\ 0 & K_{yy} & 0 \\ 0 & 0 & K_{zz} \end{bmatrix}$$

= Conductivity matrix ….(2)

Combining equations (1) and (2),

$$\rho c\left(\frac{\partial T}{\partial t} + \{v\}^T \{L\}T\right) = \{L\}^T([D]\{L\}T) + \ddot{q}$$

….. (3)

Expanding equation (3) to its more familiar form:

$$\rho c\left(\frac{\partial T}{\partial t} + v_x \frac{\partial T}{\partial x} + v_y \frac{\partial T}{\partial y} + v_z \frac{\partial T}{\partial z}\right) = \ddot{q} + \frac{\partial}{\partial x}\left(K_x \frac{\partial T}{\partial x}\right) + \frac{\partial}{\partial y}\left(K_y \frac{\partial T}{\partial y}\right) + \frac{\partial}{\partial z}\left(K_z \frac{\partial T}{\partial z}\right)$$

….(4)

It will be assumed that all effects are in the global Cartesian system.

Three types of boundary conditions are considered. It is presumed that these cover the entire element.

1. Specified temperatures acting over surface S_1:

   $$T = T^*$$ …. (5)

   where T* is the specified temperature

2. Specified heat flows acting over surface S_2:

   $$\{q\}^T\{\eta\} = -q^*$$ … (6)

   where:

   {η} = unit outward normal vector

   q* = specified heat flow.

3. Specified convection surfaces acting over surface S_3 (Newton's law of cooling):

   $$\{q\}^T\{\eta\} = h_f(T_S - T_B)$$ …..(7)

where: h_f = film coefficient, evaluated at $(T_B + T_S)/2$ unless otherwise specified for the element,

T_B = bulk temperature of the adjacent fluid, and

PDF created with pdfFactory Pro trial version www.pdffactory.com

T_S = temperature at the surface of the model.

Note that positive specified heat flow is into the boundary (i.e., in the direction opposite of {η}), which accounts for the negative signs in equations (6) and (7).

Combining equation (2) with equations (6) and (7) yields:

$$\{\eta\}^T[D]\{L\}T = q^* \quad \ldots. (8)$$

$$\{\eta\}^T[D]\{L\}T = h_f(T_B - T) \quad \ldots.(9)$$

Pre - multiplying equation (3) by a virtual change in temperature, integrating over the volume of the element, and combining with equations (8) and (9) with some manipulation yield:

$$\int_{vol}\left(\rho c\,\delta T\left(\frac{\partial T}{\partial t} + \{v\}^T\{L\}T\right) + \{L\}^T(\delta T)([D]\{L\}T)\right)d(vol) = \int_{S_2}\delta T\,q^* d(S_2) + \int_{S_3}\delta T\,h_f(T_B - T)d(S_3) + \int_{vol}\delta T\,\ddot{q}\,d(vol) \quad \ldots.(10)$$

where: vol = volume of the element, and

δT = an allowable virtual temperature (= δT (x, y, z, t)).

Expanding the Stefan-Boltzmann Law to a two-surface radiation equation, the heat transfer rate between two surfaces i and j is:

$$Q_i = \sigma\,\varepsilon_i F_{ij} A_i (T_i^4 - T_j^4) \quad \ldots.(11)$$

where:

Q_i = heat transfer rate from surface,

σ = Stefan-Boltzmann,

ε_i = effective emissivity,

F_{ij} = view factor from surface I to surface j,

A_i = area of surface i, and

T_i , T_j = absolute temperature at surface i and surface j, respectively.

Description of the Problem

The finite element program ANSYS (V 5.4) has been used in this study to simulate the flexible pavement under mechanical loads (traffic load applied) and thermal load conditions (temperature field). A schematic representation of flexible pavement is shown in Figure 8 which consists of three layers: asphalt layer, base and subgrade layer. The properties for each material are given in Table 1. Three different thicknesses for the asphalt layer were tried; namely, 0.05 m, 0.10 m and 0.15 m, respectively. The finite element work was carried out through the following stages:

1. Generation of the finite element mesh and defining the load, boundary conditions and material properties as shown in Figure 8. The mesh consists of fine elements near the loaded area and at the asphalt layer interface. The left and right vertical boundaries are constrained to move only in vertical direction whereas those on bottom boundary are all fixed.

PDF created with pdfFactory Pro trial version www.pdffactory.com

The rest nodal points including those on surface are unconstrained as shown in Figure 8.

2. The subgrade layer is modeled as elasto-plastic material following Drucker–Prager model for yielding of the isotropic material, while both the asphalt and base layers are considered elastic. A plane 42, 2-D structural solid has been adopted in this research. The element can be used as a plane element (plane strain or plane stress) or as an axis symmetric element. The element is defined by four nodes having two degrees of freedom at each node, translations and the nodal x and y directions. The element has plasticity, and large strain capability. Therefore a stiffness elastic modulus (E) and Poisson's ratio (ν), cohesion (c), angle on internal friction (ϕ) are used to represent their behavior. The coefficient of thermal linear expansion is used to model thermal behavior. Temperature dependent stiffness modulus is used for the asphalt layer. The coefficient of thermal expansion for the asphalt material is $4x10^{-4}$ /^{o}C, (Huang, 1993). A temperature rise of 40 ^{o}C was considered.
3. Computing strains, stresses displacements and stress intensity.

Contact pressures

The well known dual tire configuration is used all over the world for the driven and towed axles. Normally these tires have an inflation pressure of around 700 kPa. The steering axle of a truck always has a single tire, having the same dimensions as one of the dual tires. In Western Europe however, most of the towed axles are equipped nowadays with a so called wide base or super single tire. Normally the tire has an inflation pressure of 800 – 850 kPa. The super single tire is still under development but will be used under the driven axle of trucks thereby replacing the dual wheel configuration. In between the super single and the dual wheel is a small size dual wheel. This tire is not very much used yet. The idea behind it was that a smaller size tire would allow lowering the loading platform resulting in a larger loading capacity. In order to avoid excessive wear to the tire, the tire pressure should be selected in relation to the tire load. The following relationships can be used for this. The pressure used in the tires for dual wheels (1 axle has two dual wheels on either side of the axle; total number of wheels = 4) can be estimated from (Molenaar, 2007):

$$p = 0.35 + 0.0035\,L \qquad \ldots.(12)$$

where: p = tire pressure (MPa), and
L = axle load (kN).

The pressure in the super single tires (1 axle has one wheel on either side of the axle; total number of wheels = 2) can be estimated using:

$$p = 0.42 + 0.0038\,L \qquad \ldots. (13)$$

In this paper, the pressure caused by axles was calculated using equations

PDF created with pdfFactory Pro trial version www.pdffactory.com

(12) and (13). They were 500, 700 and 1000 kN/m^2.

Results and Discussion

Figures 9, 10 and 11 show the surface settlement under the effect of loads without considering temperature effects. It can be noticed that a considerable increase in settlement takes place under the wheels when the wheel pressure increases from 500 to 700 and 1000 kN/m^2. As the thickness of the asphalt layer increses from 0.05 m to 0.10 m, an increase in displacement of the order of about (61-73%) is noticed. This increase becomes about (122-147%) when the thickness is incresed to 0.15 m. In Figure 10, the case of temperature effect (no load) is presented. It can be noticed that the temperature causes uniform deformation in the layers which was about (21.6 mm). The same effect was found when the thickness of asphalt layer was changed to (0.10) or (0.15) m.

In these figures, the magnitude of wheel pressure is important. An increase of wheel pressure from (500) to (700) kN/m^2 leads to increase in vertical displacement of about (4 – 8)%. This increase becomes (10– 22%) when the wheel pressure becomes 1000 kN/m^2.

It can be noticed that under the locations of wheels, the deformation takes the form of ruttings.

Figure 12 illustrates the distribution of vertical displacement in the road layers under the effect of temperature rise of 40^{o}C only. It can be seen that the maximum uniform displacement is about (0.0216 m). This leads to the conclusion that the temperature rise leads to decrease in the effect of wheel pressure because temperature leads to expansion (upward movement) reverse to wheel load effect.

Figures 13 to 15 show the deformed layers of road under the effect of wheel pressure and temperature rise when the asphalt layer thickness is 0.05 m. It is apparent that the effect of wheel load is transmitted directly to the underlying subgrade within the wheel zone. The deformed zone under the wheel becomes larger when the load increases. The maximum displacement increases by about (24%) when the load is duplicated.

This was also concluded from Figures 16 to 18 for asphalt layer thickness of 0.1 m and Figures 19 to 21 for asphalt layer thickness of 0.15 m.

Figures 22 to 24 present the distribution of deviator stress (principal stress difference σ_1 - σ_3) in the subgrade layer. It can be noticed that the increase of wheel pressure leads to increase in deviator stresses within the wheel zone and hence, the probability of failure in these zones becomes larger. The increase of asphalt layer thickness decreases the loads transmitted to the subgrade layer. It is evident in these figures that when the wheel pressure reaches (1000 kN/m^2), the maximum deviator stress exceeds the strength of the subgrade layer and hence failure is expected.

Conclusions

1. The temperature causes uniform deformation in the layers which was about (21.6 mm). The same

PDF created with pdfFactory Pro trial version www.pdffactory.com

effect was found for all thicknesses of the asphalt layer (0.05), (0.10) or (0.15) m.

2. An increase of wheel pressure from (500) to (700) kN/m^2 leads to increase in vertical displacement of about (4 – 8)%. This increase becomes (10 – 22%) when the wheel pressure becomes 1000 kN/m^2. The temperature rise leads to decrease in the effect of wheel pressure because temperature leads to expansion (upward movement) reverse to wheel load effect.
3. The effect of wheel load is transmitted directly to the underlying subgrade within the wheel zone. The deformed zone under the wheel becomes larger when the load increases. The maximum displacement increases by about (24%) when the load is duplicated.
4. The increase of asphalt layer thickness decreases the loads transmitted to the subgrade layer. When the wheel pressure reaches (1000 kN/m^2), the maximum deviator stress exceeds the strength of the subgrade layer and hence failure is expected.

References

- Alkaiss, Z. A. and Al-Maliky, S. E. S., "Combined effect of wheel and thermal load conditions on stress distribution in flexible pavement", Engineering and Technology Journal, University of Technology, Vol. 27, No. 12, p.p. 2257-2267, 2009.
- "ANSYS Manual", Version (5.4), USA, 1996.
- Van Gurp, C.A.P.M.; "Characterization of seasonal influences on asphalt pavements with the use of falling weight deflectometers", Ph.D. Dissertation Delft University of Technology. Delft, 1995.
- Huang, H.Y. ; "Pavement Analysis and Design". Prentice-HALL, Englewood Cliffs, New Jersey, 1993.
- Lytton, R.L.; "Use of geotextiles for reinforcement and strain relief in asphalt concrete", Geotextiles and Geomembranes, Vol. 8, No. 3. 1989.
- Molenaar, A. A. A., "Lecture notes ct 4860 structural pavement design-design of flexible pavements", Delft, March 2007.
- Pavement Design Manual, Issued by the Queensland Department of Main Roads, Pavements, Materials & Geotechnical Division, State of Queensland, Department of Main Roads, 2005.

PDF created with pdfFactory Pro trial version www.pdffactory.com

Table (1) Material properties for the pavement layers materials, (Huang, 1993).

Material Name	Modulus of Elasticity, E (kN/m^2)	Poisson's Ratio, n	Cohesion, c (kN/m^2)	Angle of Friction, f (Degrees)
Asphalt	**51.7×10^3**	**0.35**	**-**	**-**
Base	**103.5×10^3**	**0.30**	**-**	**-**
Subgrade	**135.3×10^3**	**0.40**	**158**	**0**

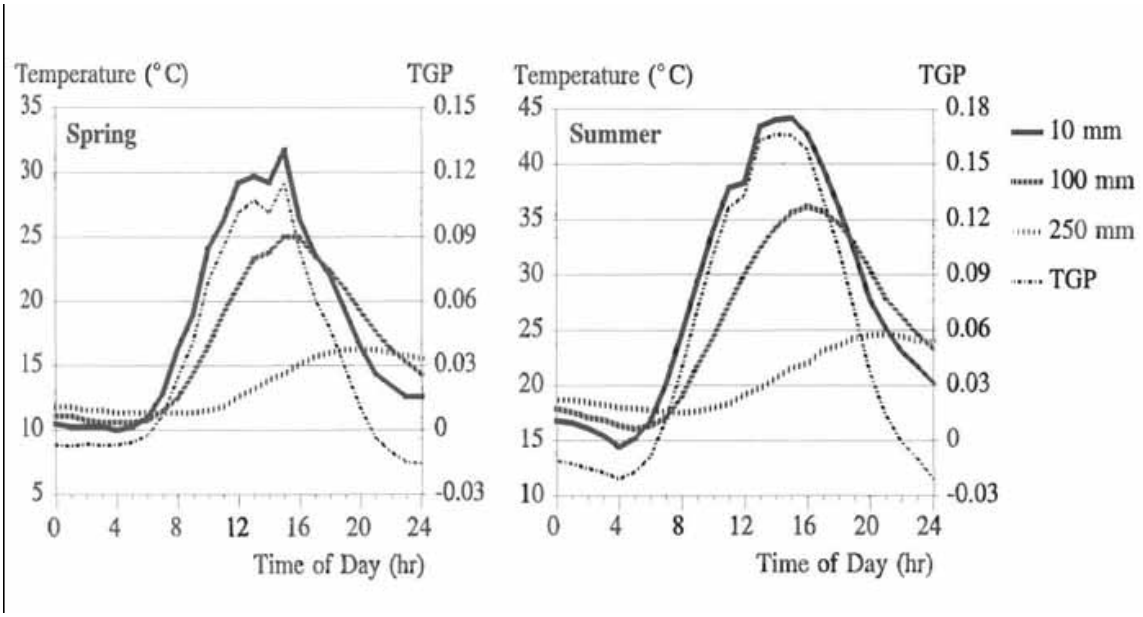

Figure (1) Temperature variations during the day over the thickness of the asphalt pavement, (Molenaar, 2007).

PDF created with pdfFactory Pro trial version www.pdffactory.com

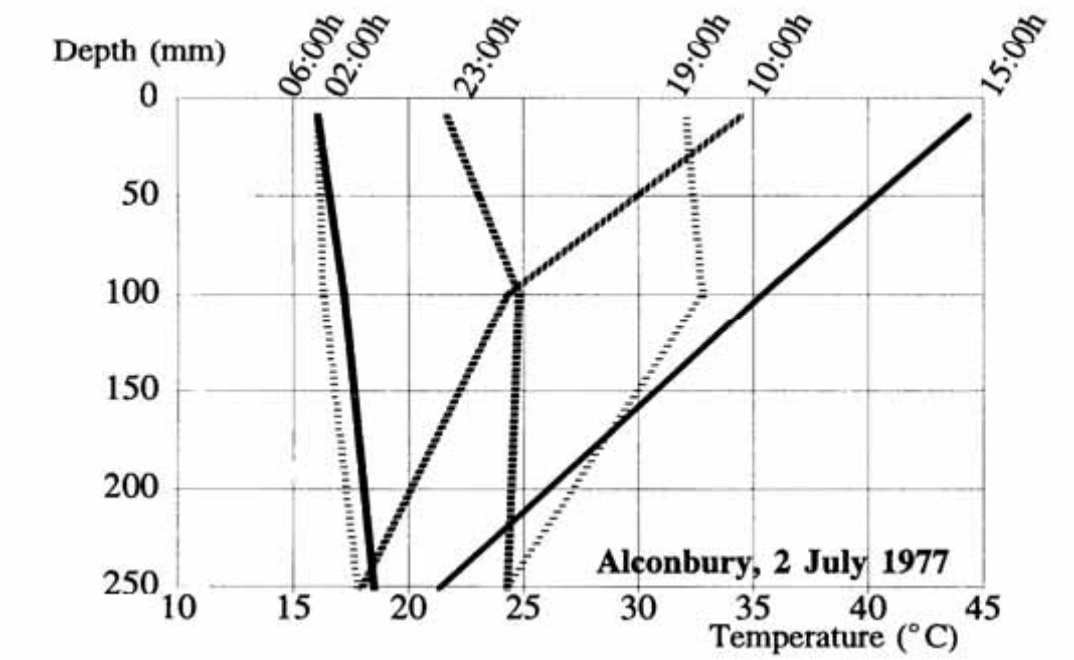

Figure (2) Temperature gradient in an asphalt pavement on a hot summer day, (Molenaar, 2007).

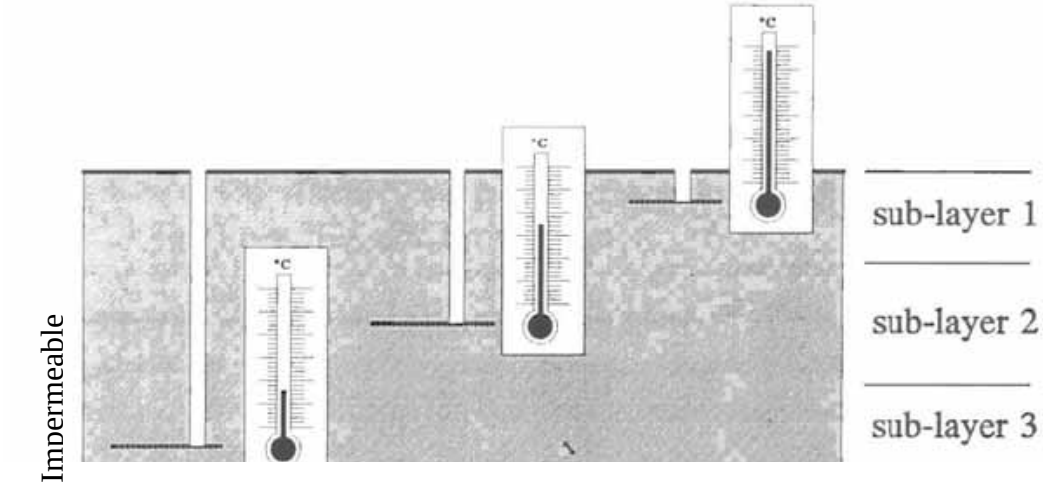

Figure (3) Dividing the total asphalt thickness in sub-layers.

PDF created with pdfFactory Pro trial version www.pdffactory.com

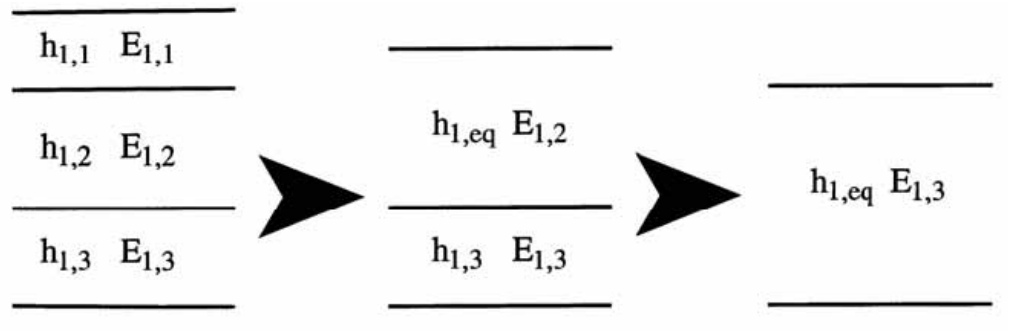

Figure (4) Calculation of the equivalent asphalt thickness $h_{1,eq}$, (Molenaar, 2007).

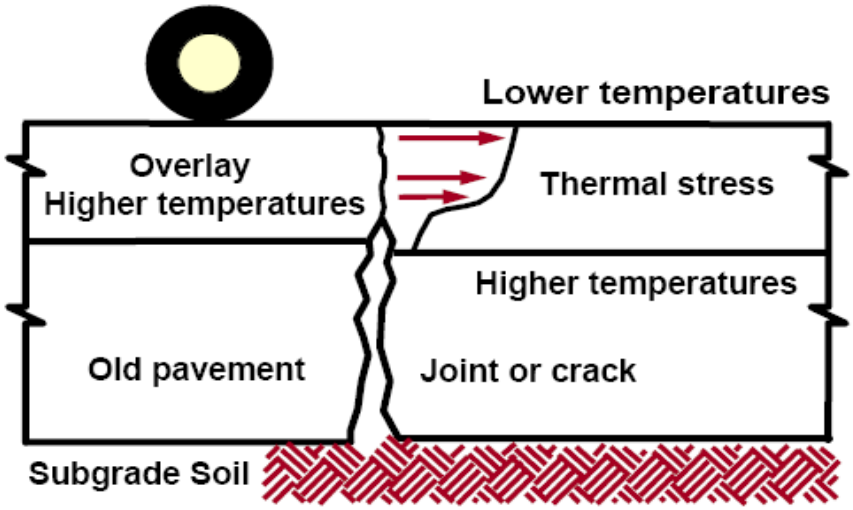

Figure (5) Crack reflection because of shrinkage of the base, (Molenaar, 2007).

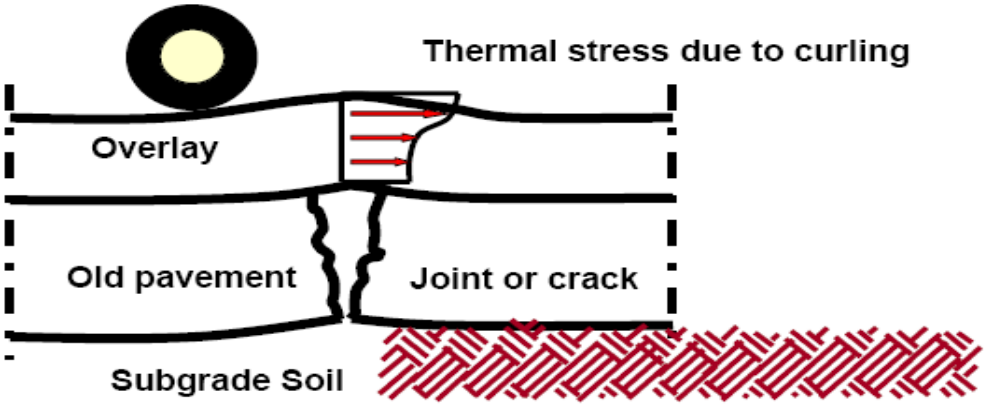

Figure (6) Crack reflection due to curling of the cement treated base, (Molenaar, 2007).

PDF created with pdfFactory Pro trial version www.pdffactory.com

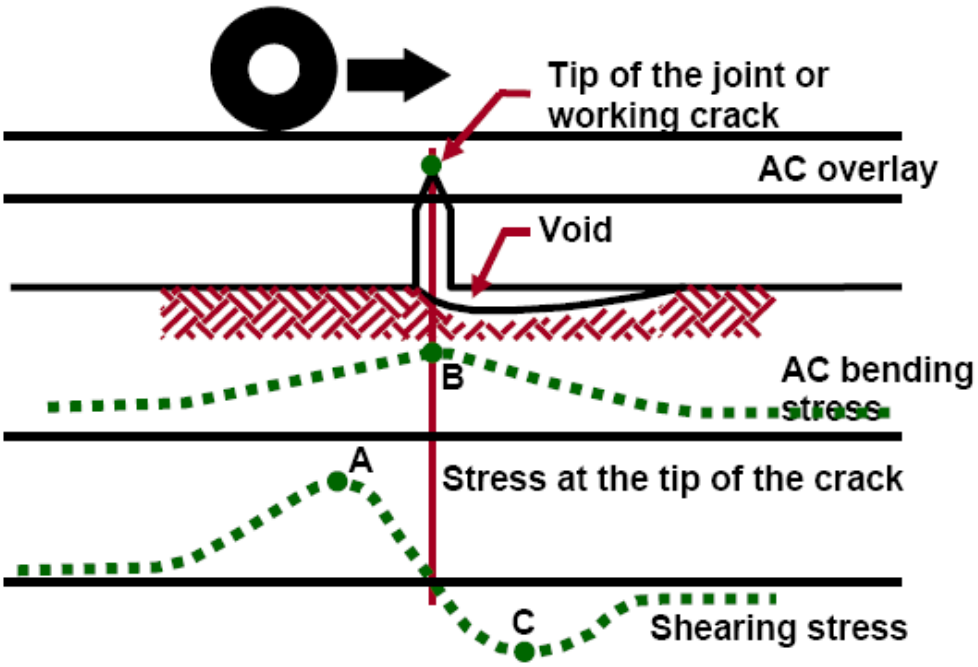

Figure (7) Crack reflection due to traffic loads, (Molenaar, 2007).

PDF created with pdfFactory Pro trial version www.pdffactory.com

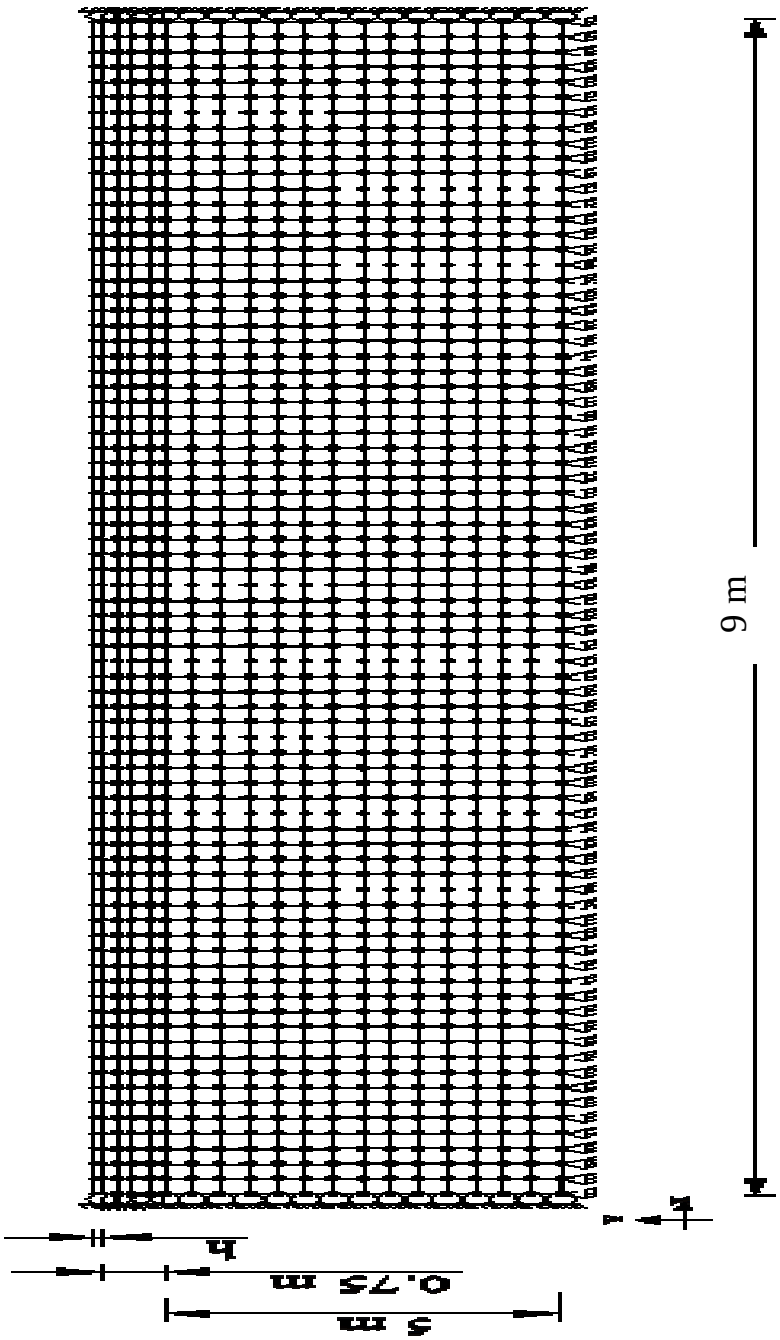

Figure (8)The finite element mesh

PDF created with pdfFactory Pro trial version www.pdffactory.com

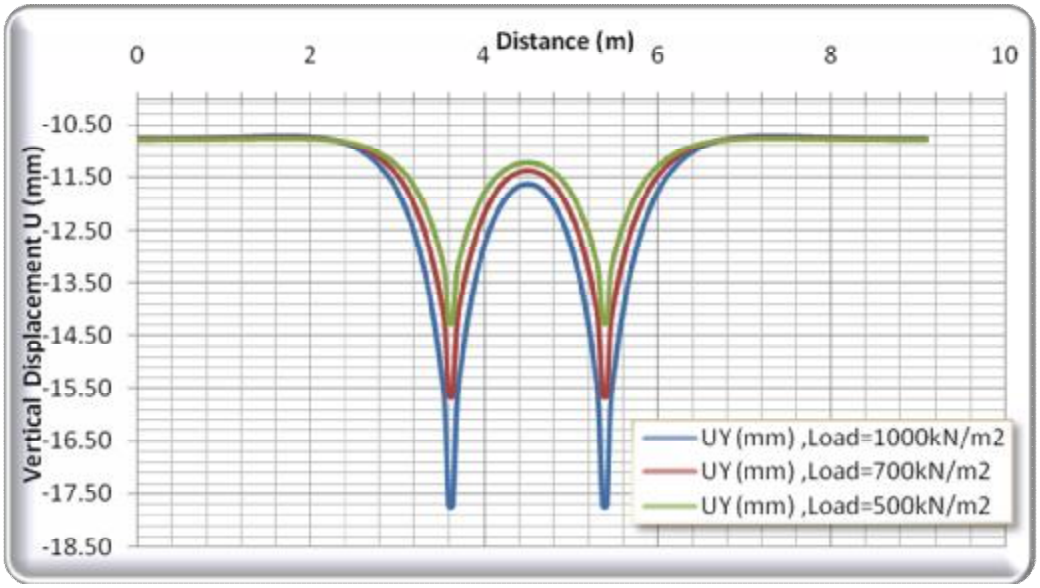

Figure 9: Surface settlement of the asphalt layer under different wheel pressures when the thickness is 0.05 m.

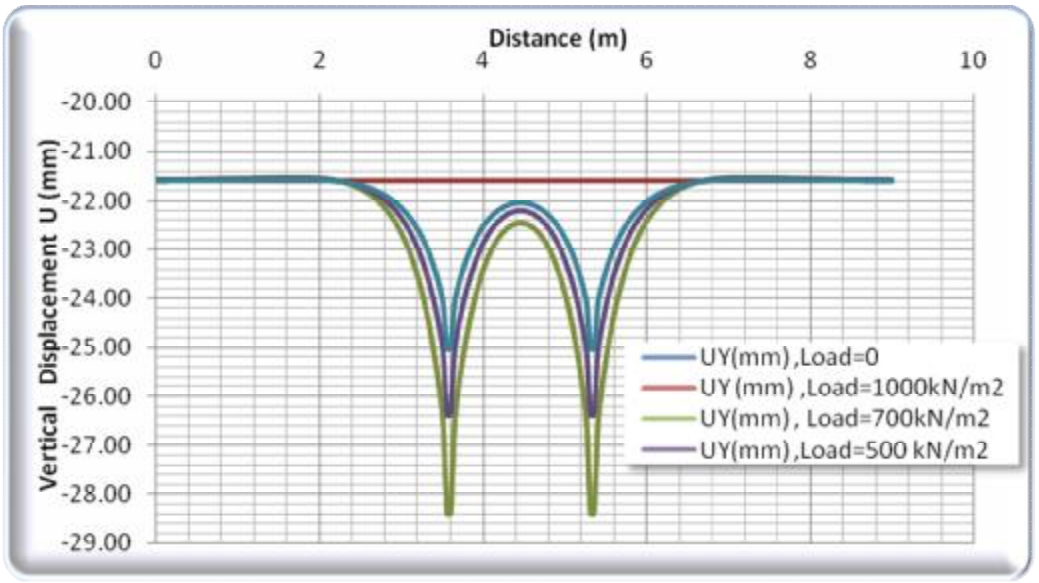

Figure 10: Surface settlement of the asphalt layer under different wheel pressures when the thickness is 0.10 m.

PDF created with pdfFactory Pro trial version www.pdffactory.com

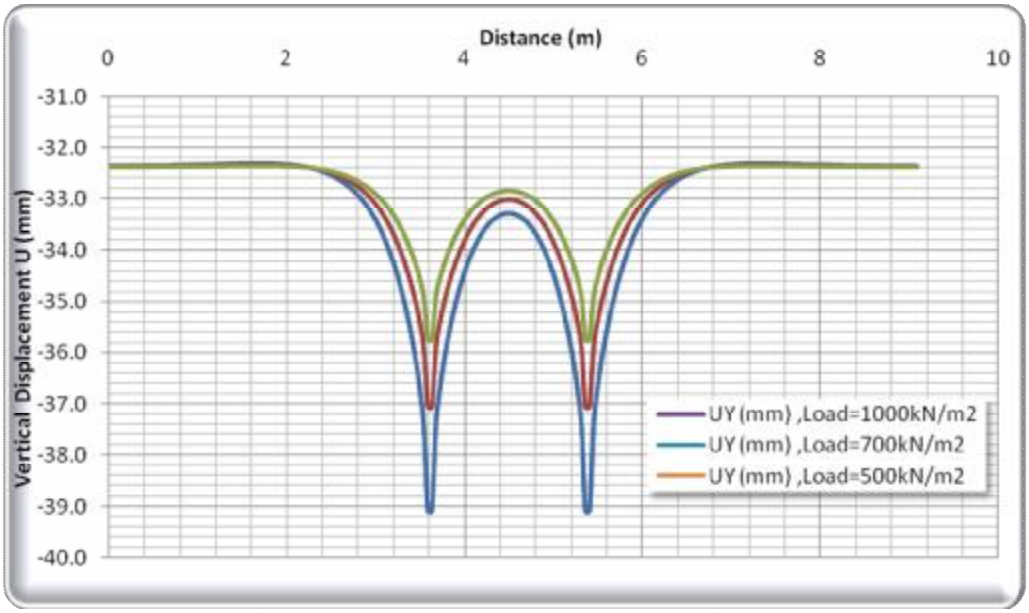

Figure 11: Surface settlement of the asphalt layer under different wheel pressures when the thickness is 0.15 m.

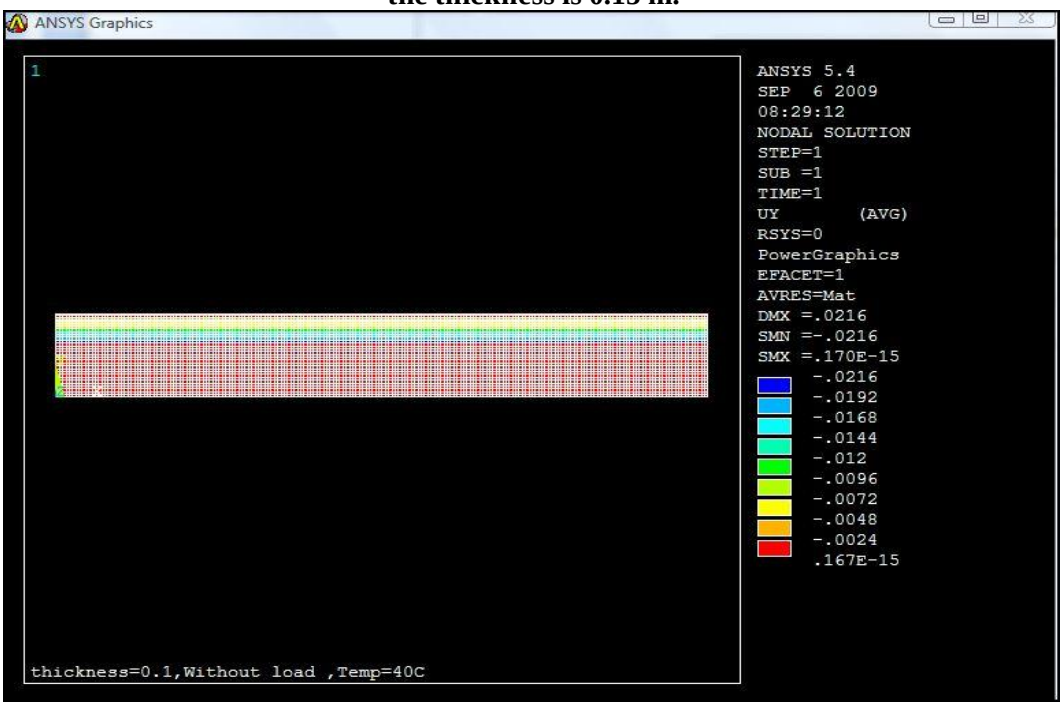

Figure 12: Distribution of vertical displacement in the road layers under the effect of temperature rise of 40ºC when the thickness is 0.05 m.

PDF created with pdfFactory Pro trial version www.pdffactory.com

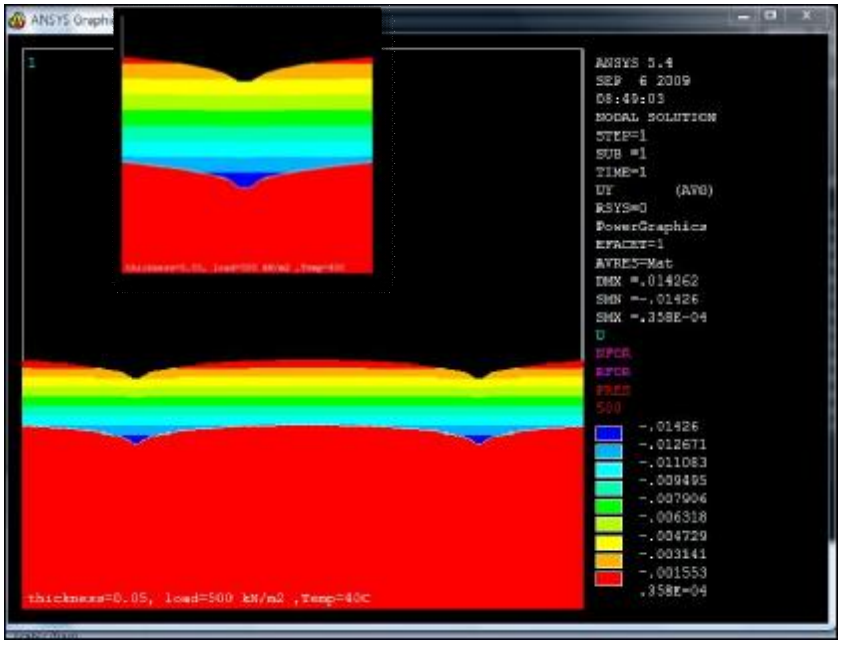

Figure 13: Distribution of vertical displacement in the road layers under the effect of wheel pressure = 500 kN/m^2 and temperature rise of 40^{0}C when the thickness is 0.05 m.

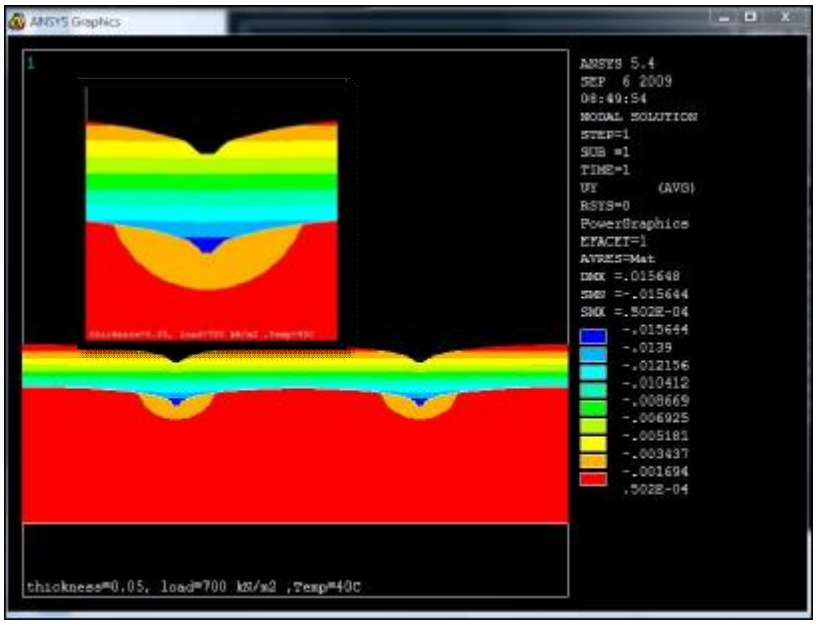

Figure 14: Distribution of vertical displacement in the road layers under the effect of wheel pressure = 700 kN/m^2 and temperature rise of 40^{0}C when the thickness is 0.05 m.

PDF created with pdfFactory Pro trial version www.pdffactory.com

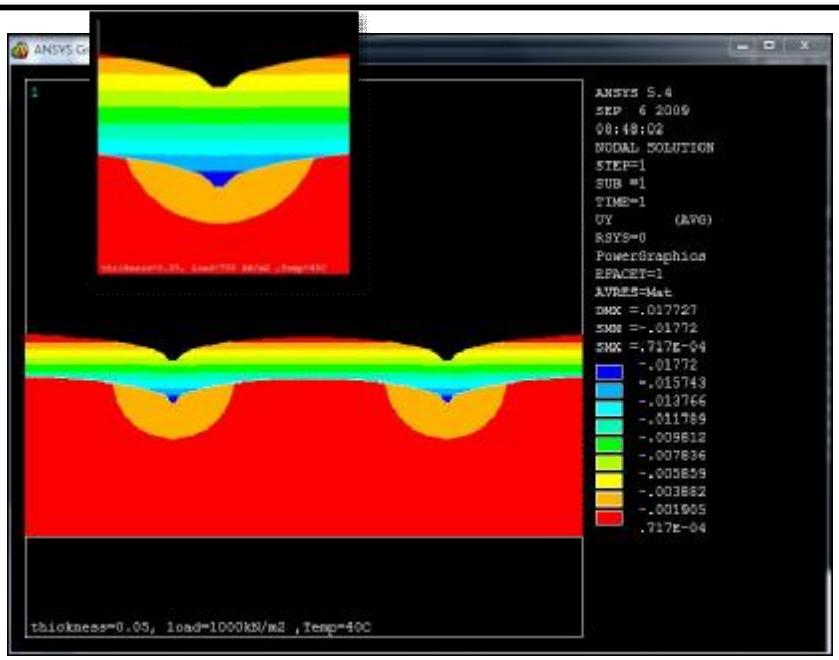

Figure 15: Distribution of vertical displacement in the road layers under the effect of wheel pressure = 1000 kN/m^2 and temperature rise of 40^{0}C when the thickness is 0.05 m.

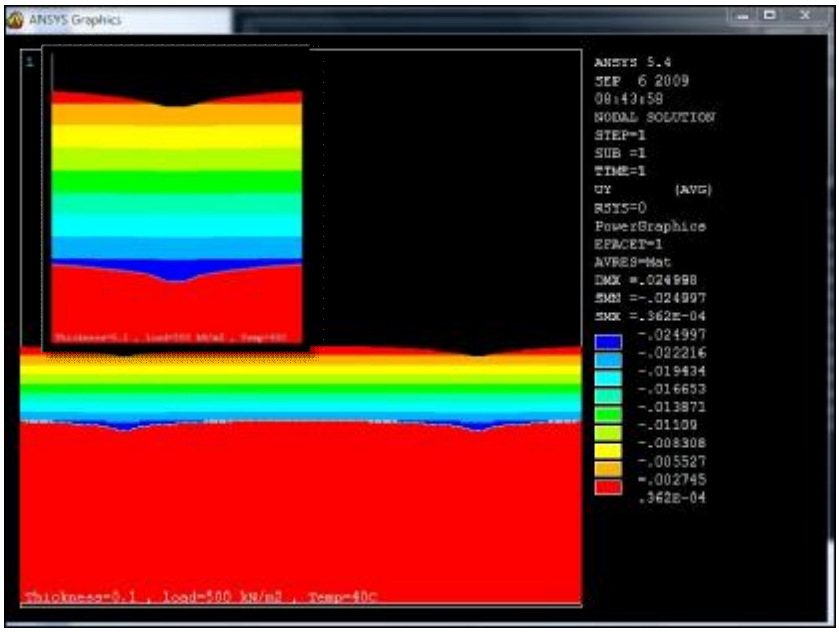

Figure 16: Distribution of vertical displacement in the road layers under the effect of wheel pressure = 500 kN/m^2 and temperature rise of 40^{0}C when the thickness is 0.10 m.

PDF created with pdfFactory Pro trial version www.pdffactory.com

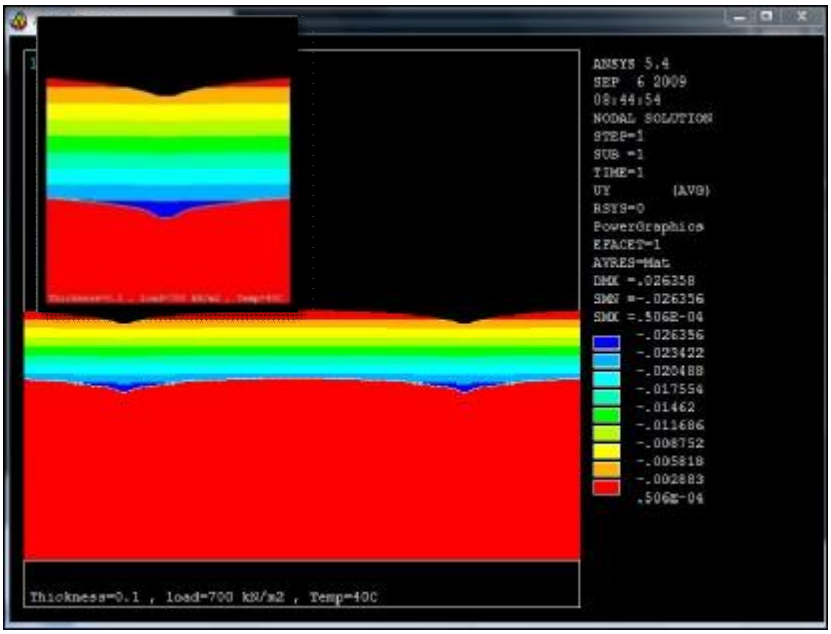

Figure 17: Distribution of vertical displacement in the road layers under the effect of wheel pressure = 700 kN/m^2 and temperature rise of 40^{0}C when the thickness is 0.10 m.

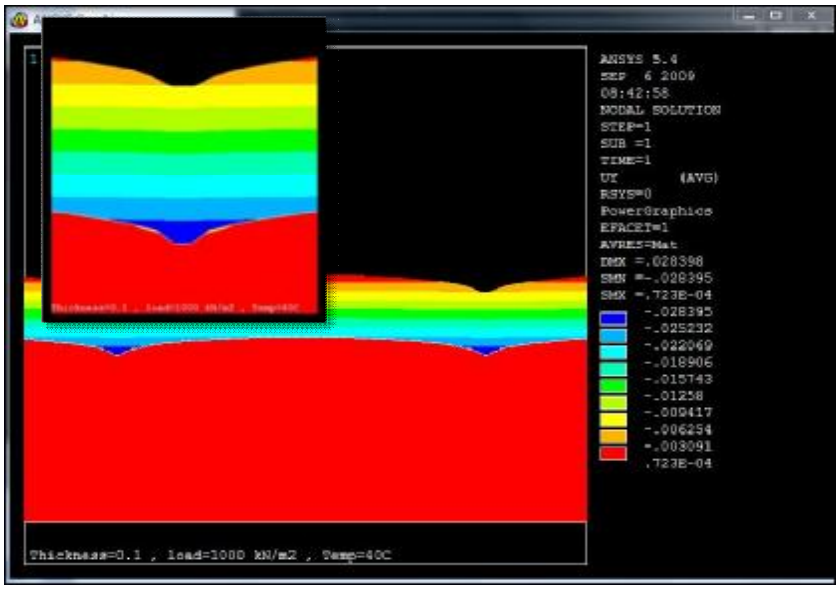

Figure 18: Distribution of vertical displacement in the road layers under the effect of wheel pressure = 1000 kN/m^2 and temperature rise of 40^{0}C when the thickness is 0.10 m.

PDF created with pdfFactory Pro trial version www.pdffactory.com

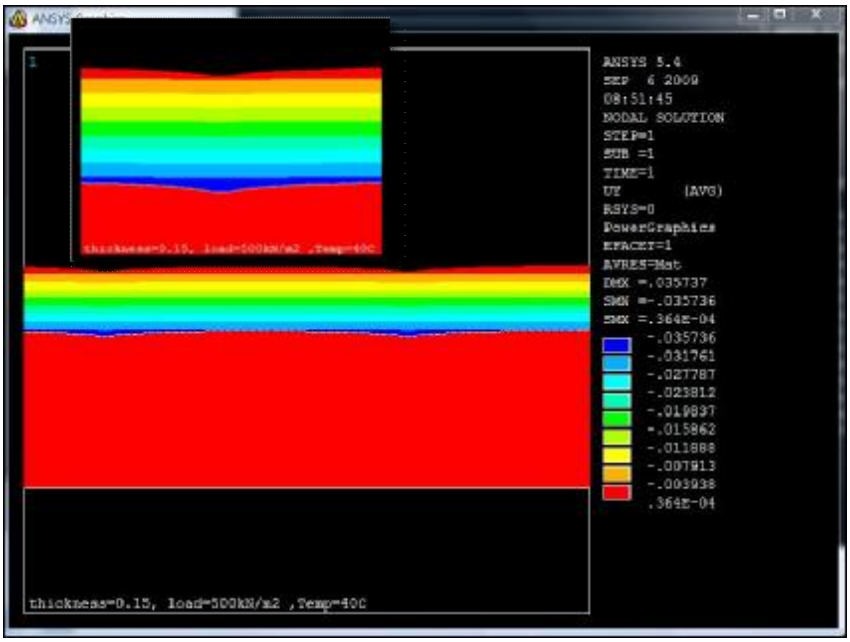

Figure 19: Distribution of vertical displacement in the road layers under the effect of wheel pressure = 500 kN/m^2 and temperature rise of 40^{0}C when the thickness is 0.15 m.

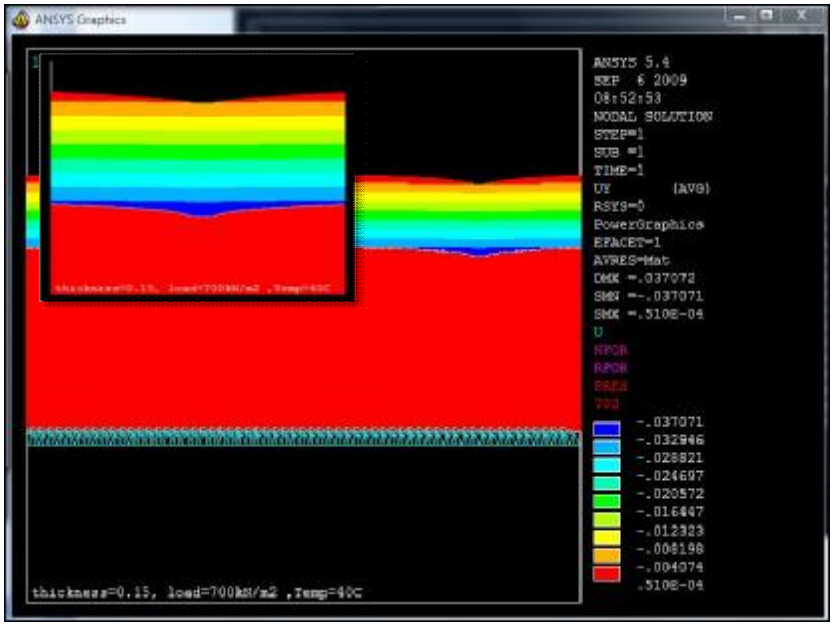

Figure 20: Distribution of vertical displacement in the road layers under the effect of wheel pressure = 700 kN/m^2 and temperature rise of 40^{0}C when the thickness is 0.15 m.

PDF created with pdfFactory Pro trial version www.pdffactory.com

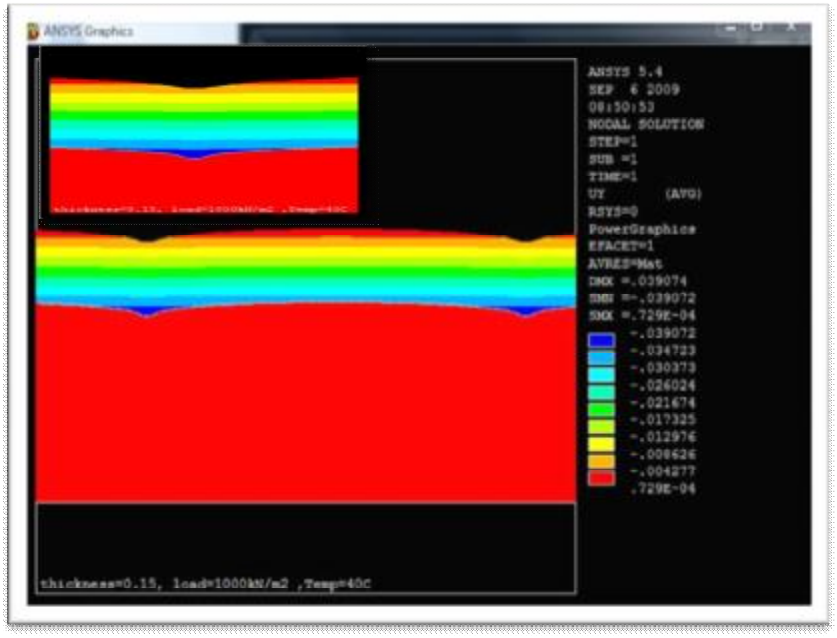

Figure 21: Distribution of vertical displacement in the road layers under the effect of wheel pressure = 1000 kN/m^2 and temperature rise of 40^{0}C when the thickness is 0.15 m.

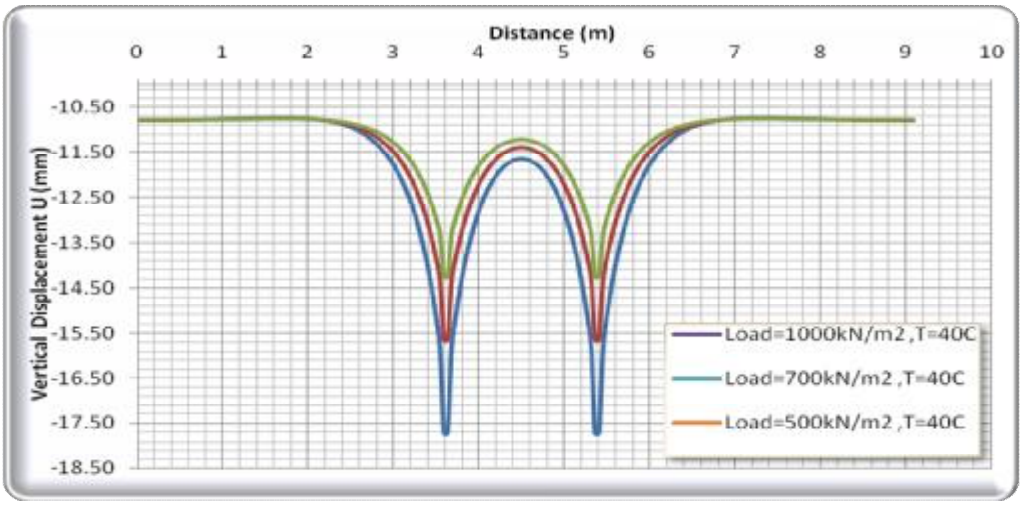

Figure 22: Distribution of the maximum deviatoric stress in the subgrade layer under the effect of different wheel pressures and temperature rise of 40^{0}C when the thickness is 0.05 m

PDF created with pdfFactory Pro trial version www.pdffactory.com

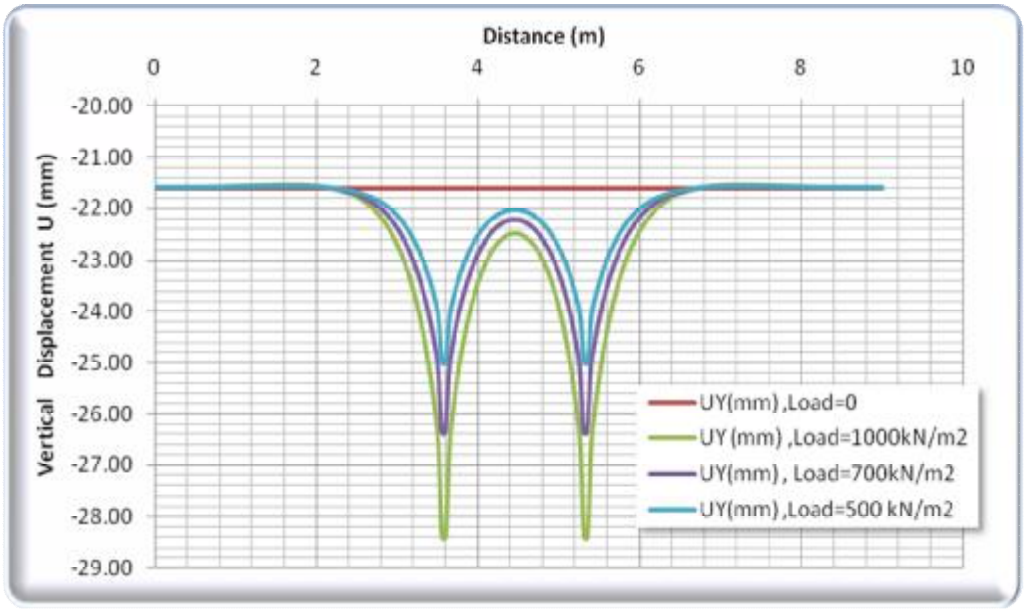

Figure 23: Distribution of the maximum deviatoric stress in the subgrade layer under the effect of different wheel pressures and temperature rise of 40C when the thickness is 0.10 m.

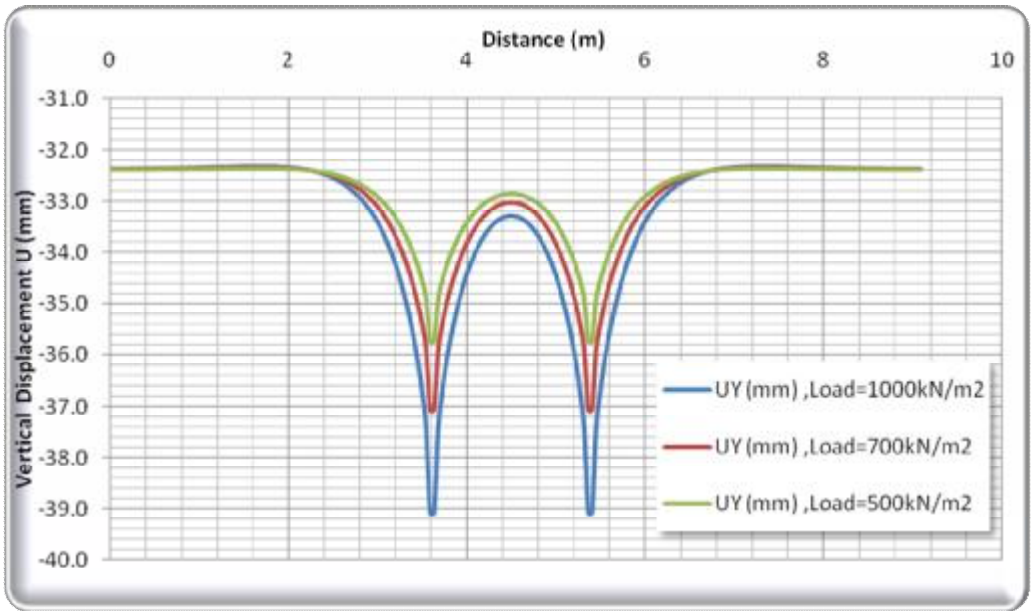

Figure 24: Distribution of the maximum deviatoric stress in the subgrade layer under the effect of different wheel pressures and temperature rise of 40C when the thickness is 0.15 m.

PDF created with pdfFactory Pro trial version www.pdffactory.com